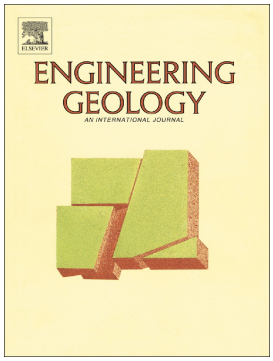

Stratigraphy, petrophysical characterization and 3D geological modelling of the historical quarry of Nueva Tabarca island (western Mediterranean): Implications on heritage conservation

J. Martínez-Martínez, H. Corbí, I. Martin-Rojas, J.F. Baeza-Carratalá, A. Giannetti

PII:	S0013-7952(17)30875-X
DOI:	doi:10.1016/j.enggeo.2017.10.014
Reference:	ENGEO 4679
To appear in:	*Engineering Geology*
Received date:	9 June 2017
Revised date:	14 September 2017
Accepted date:	18 October 2017

Please cite this article as: J. Martínez-Martínez, H. Corbí, I. Martin-Rojas, J.F. Baeza-Carratalá, A. Giannetti , Stratigraphy, petrophysical characterization and 3D geological modelling of the historical quarry of Nueva Tabarca island (western Mediterranean): Implications on heritage conservation. The address for the corresponding author was captured as affiliation for all authors. Please check if appropriate. Engeo(2017), doi:10.1016/j.enggeo.2017.10.014

Stratigraphy, petrophysical characterization and 3D geological modelling of the historical quarry of Nueva Tabarca island (western Mediterranean): implications on Heritage Conservation

Martínez-Martínez, J.[1,2], Corbí, H.[1], Martin-Rojas, I.[1], Baeza-Carratalá, J.F.[1], Giannetti, A.[1]

[1] Departamento de Ciencias de la Tierra y del Medio Ambiente. Universidad de Alicante. Campus San Vicente del Raspeig. 03690 San Vicente del Raspeig (Alicante, Spain).
[2] Instituto Geológico y Minero de España (IGME). Calle Ríos Rosas, 23. 28003 Madrid (Spain)

Abstract

The historical quarry of the Nueva Tabarca fortress (Mediterranean Sea, SE of Spain) was developed in a complex sedimentary Miocene deposit. Five lithostratigraphic units have been defined, including different lithologies such as breccias and microconglomerates (Unit 1), massive and laminated lithoarenites (Units 1, 3 and 5), calcarenites and biocalcirudites (Units 2 and 4). A complete stratigraphic description of this sequence has been carried out, as well as the petrophysical characterization of the most significant lithologies including the analysis of rock durability as well as hydraulic and mechanical properties. Regarding durability, the softest rocks correspond to those from the Unit 4, whilst samples from Units 2 and 5 are the most durable. Three weathering patterns were observed during the artificial ageing test according to both the velocity and intensity of the sample decay. Each pattern is explained according to water-circulation possibility through the rock, its porous system, and the mechanical strength. Rock weathering in monuments of Nueva Tabarca is quantified and discussed according to the results found in the laboratory. Several decay forms are observed in the building stones (mainly differential erosion, alveolization, and rounding forms). Both 3D photogrammetric and 3D geological model of the historical quarry were elaborated in order to quantify the extracted volume of building stones, differentiating the specific quarried percentage of each lithology. Correlation between the results obtained in the volumetric analysis of the historical quarry and the building stones used in the monuments has been carried out. 3D models were also used for determining the remaining rock volume in the current outcrops. Finally, a set of recommendations for future conservation works of the architectural heritage are proposed after the current availability of the different rock varieties and their petrophysical behaviour.

Key words: photogrammetry, durability, weathering, building stone, Nueva Tabarca island

1. Introduction

The location and study of historical quarries is a fundamental task for the restoration of a monument. When the stones in monuments are deeply weathered, they require replacement by new ones. However, the use of inappropriate replacement stones can result in significant damage to the heritage. The literature shows the problems resulting from the use of inadequate replacement stones (Sasse and Snethlage, 1996; Dreesen and Dusar, 2004; Hyslop, 2004; Rozenbaum et al., 2008; Graue et al., 2011). Therefore, the choice of the replacement stone should be appropriate in physical and aesthetic terms and, ideally, it should be of the same type as the original building stone, or the nearest possible equivalent (Pereira and Marker, 2016). Therefore, knowing the location of original stone source, as well as the petrographical and petrophysical properties of the rock, helps guarantee effective restoration work. Consequently, the interest of research groups in historical quarries has been increasing in recent years (Cooper, 2010; Hyslop et al., 2010; Fronteau et al., 2010; Baltuille et al., 2012; Pereira et al., 2013).

It is generally accepted that the main physical properties for stone compatibility include their hydro-mechanical performance in terms of properties such as water absorption, capillarity or mechanical strength, which in turn depend on the porous system of the rock (Andriani and Walsh, 2003; Rozenbaum et al., 2008). The pore network of building stones, and consequently, most of their petrophysical properties, is strongly related to the microfacies of the source rock (i.e. to their sedimentary and diagenetic history). Hence, a full characterization requires a multi-perspective approach to understand the natural variability of stone resources (Bednarik et al., 2014; De Kock et al., 2017). Rock microfacies can be relatively constant over large bodies of rock or they can fluctuate strongly on a subcentimetre to decimetre scale (De Kock et al., 2017). Consequently, it is essential to have accurate knowledge of the stratigraphic sequence (in sedimentary rocks) as well as the geometry of the rock bodies and their spatial distribution. The combination of traditional geological work with new photogrammetry techniques enables a highly precise 3D outcrop characterization. In these terms, the historical quarry of Nueva Tabarca island constitutes an exceptional study case due to the lithological variations throughout the stratigraphic sequence and the volumetric distribution of the regular and irregular layers.

The fortified village of Nueva Tabarca constitutes an valuable example of homogeneous baroque architectural heritage (Beviá and Giner Martínez, 2008). The singularity of the monuments was recognized by several local and national protective measures. The initial plans for this fortified city were focused on the building of a strong wall around the west part of the island and the construction of several buildings with military, religious, and civil functions. The reason for this important intervention was to offer a stronger resistance against the Barbary pirates. The construction works began in the mid 18th century, and were stopped in 1770, due to economic, political, and logistical problems. The result was the construction of most of the wall, the church, the governor's house and a complex hydraulic system in order to supply the population with fresh water. Due to the insularity conditions, the supply of the building materials was restricted to the local resources. In this context, the most appropriate rock for carving the ashlars and sculptural elements was a yellowish calcarenite which outcrops in one

of the rocky islets surrounding the main island (*La Cantera* islet, which means "the quarry" in Spanish).

Unfortunately, the current conservation state of the city-walls and buildings is alarming. The sea-salt crystallization in the porous system of rocks, the wind abrasion, and human damage are some of the most significant decay causes. On the other hand, not all the materials present the same weathering resistance. Despite that the whole rock blocks were extracted from the same local quarry, several lithofacies can be recognised and each presents different petrophysical and petrographical properties. As a result, the 3D geological characterization of the historical quarry is extremely useful for determining the current susceptibility of monuments to weathering as well as for establishing a petrophysical criterion to select the best replacement stones for future restoration.

The aim of this paper is the geological characterization of the historical quarry of Nueva Tabarca island from a multi-perspective point of view. The main points in this study are: i) the determination of the complete stratigraphic section of the Miocene deposits outcropping in the island; ii) the modelling of the 3D spatial distribution of the different lithostratigraphic units of the *La Cantera* islet; iii) the petrophysical characterization of the main lithotypes recognized in the islet; and iv) the correlation of the data gathered from the volumetric analysis and the petrophysical characterization with the weathering state observed in the rocks of the architectural heritage of the Nueva Tabarca fortress.

2. Geological setting

The Betic Cordillera makes up the westernmost part of the Mediterranean Alpine chains. It spreads along more than 600 km, in the south-eastern part of the Iberian Peninsula (figure 1). Two great geological realms are distinguished: the Internal and the External Zones. The Internal Zones are made up of three overthrusting units (Nevado-Filábride, Alpujárride, and Maláguide) which are composed mainly of Triassic and Palaeozoic rocks. The External Zones are represented by a sedimentary rock belt making up the northern sector of the chain. Neogene-Quaternary sedimentary deposits cover the Internal Zones, filling the basins developed during the extensional tectonics occurring since the early-middle Miocene.

The Bajo Segura Basin is one of the so-called post-Orogenic Neogene Basins of the Betic Cordillera (figure 1). The infill units outcropping in the Bajo Segura Basin include Tortonian to Quaternary sediments, with the strong tectonic control exerted by the Trans-Alboran shear zone, which is still active (Montenat et al., 1990; Soria et al., 2001, 2008). The sedimentary record of this basin represents one of the most complete Neogene sedimentary records of the Mediterranean margins (Soria et al., 2008a,b; Caracuel et al., 2011, García-García et al., 2011). According to Soria et al. (2008a), the marine sedimentary record of this basin is divided into five major allostratigraphic units (synthems) with bounding unconformities represented by erosional surfaces that correspond to palaeogeographic and tectosedimentary changes (Tortonian I, Tortonian II, Tortonian-Messinian I, Messinian II, and Pliocene).

Nueva Tabarca island is located in the eastern sector of the Internal Zones of the Betic Cordillera (figure 1). The main rocks observed in the island are: fine-grained metagabbro (weakly metamorphosed), marl, black limestone, porous limestone (calcarenite), red silt and marine conglomerate. According to the chronostratigraphic sequence proposed by Estévez et al. (1985), the oldest rocks correspond to the Triassic materials of the Alpujárride complex, being consequently the easternmost outcrop of this complex in the Betic Cordillera. The Triassic set is formed by the fine-grained metagabbro (constituting the base of this Triassic level), the black limestones and the marls. The calcarenites (late Miocene in age according to Kampschuur and Simon, 1969) appear in the western sector overlying an erosive unconformity with the lower Triassic materials. This sedimentary deposit forms the *Tabarca Unit* (Calvet, 1996), and is interpreted as an open carbonate platform grading upwards to more distal deposits. According to Calvet (1996), the presence of the *Globorotalia pseudomiocenica* (included in the *Globorotalia menardii* group), previously identified by Kampschuur and Simon (1969), dates these deposits as Tortonian, being included in the synthem Tortonian II of the Bajo Segura Basin (Montenat, 1977; Corbí, 2010; Corbí and Soria, 2016). Finally, the red silts and the marine conglomerates correspond to Quaternary deposits and are separated from the Triassic and Neogene sediments by an unconformity.

3. Methodology

3.1. Stratigraphic analysis

Three stratigraphic sections of the Miocene deposits were studied (figure 2): Moll Vell (MV), San Gabriel (SG) and Cantera (C) sections. The most representative stratigraphic levels were sampled bed-by-bed in order to carry out a complete petrophysical characterization at laboratory.

Description at mesoscopic level was focused on layer thickness, bed geometry, rock texture and sedimentary structures. Petrographic components and fossil record were also studied, paying special attention to the relative content between both lithoclasts and bioclasts (specially rhodoliths), as well as the medium size of the predominant component, subsequently defining lithofacies. According to these criteria, four basic lithofacies were defined. On the one hand, when the medium clast size is larger than 2 mm, the lithofacies is named *microconglomerate* when lithoclasts are predominant or *calcirudite* when bioclasts dominate. On the other hand, lithofacies with components smaller than 2 mm are classified as *biocalcarenite* or *lithoarenite* after the predominance of bioclasts or lithoclasts, respectively.

3.2. Photogrammetry and 3D geological model

Geoscientist have used photogrammetry for many years through stereoscopic analysis of overlapping pairs of aerial photographs (e.g. Eardley, 1942; Pillmore, 1964). In recent years, structure-from-motion (SfM) photogrammetry software has been providing powerful tools for geosciences (Favalli et al., 2012; Bemis et al., 2014), enabling automated 3D model production from a suite of overlapping two-dimensional images (e.g. James and Varley, 2012; Westoby et

al., 2012; James and Robson, 2014; Bemis et al., 2014). an initial limitation of this technique lay in achieving optimal camera positioning relative to the analysed outcrop. This limitation has recently been reduced by using multi-rotor unmanned aerial vehicles (UAVs), which can hover and image the outcrop from a greater range of perspectives (e.g., Smith et al., 2009; Niethammer et al., 2012; Stumpf et al., 2013). After photograph acquisition, the 3D digital outcrop model is produced by processing the images using SfM photogrammetric software. By this workflow, each point identified in multiple images is included in an outcrop model as a discrete point in 3D space. The result is a 3D cloud of points in its own photogrammetric coordinate system, which can be scaled, oriented, and positioned into a real-world coordinate system by using reference points and/or Exif metadata from images (including the location, orientation, and tilting of the camera) if available.

For a 3D photogrammetic model to be made of the historical quarry of the Nueva Tabarca island, 997 photographs were taken using a Phantom III Advanced UAV. This device includes a 12 megapixel camera with a 20 mm (35 mm equivalent) lens and a built-in unit which collects the GPS position and orientation data for each picture. These images were acquired in a series of sub-parallel continuous lines over two 1.5-hour periods under sunny conditions. Photographs were collected with 60-70% overlap between adjacent images, with a camera position orthogonal to the surface (e.g. Krauss, 1993; Abdullah et al., 2013; Micheletti et al., 2015). Three different sets of photographs were acquired at three different flight altitudes (ca. 5 m, 10 m and 30 m). To mitigate the systematic error that can be introduced across models derived from image sets where all photos are parallel collected (James and Robson, 2014), additional photographs were taken with inclined view direction. The 3D model was constructed using the software Agisoft Photoscan ©, following the standard workflow for DEM generation without ground control points (Agisoft, 2017). Key-point detection and matching aligned 908 photographs into a single 3D sparse point cloud. A subsequent dense cloud of points was computed at medium quality, resulting in a 3D model of 25.14 million points, with an average point spacing of 0.02 m. The outcrop model was converted into a real-world reference frame using the positions of the images recorded by the built-in GPS device of the aircraft.

The 3D photogrammetric model served as the basis for constructing a geological 3D model of the historical quarry of Nueva Tabarca island with the aim of computing the extracted volume of each stratigraphic unit. Input data to this model also included a georeferenced detailed geological mapping of the previously described stratigraphic units, structural data, and 49 cross sections. Cross sections were traced both perpendicular (28) and parallel (21) to the main structural direction. All these data were loaded in a Move © project, this application provides an environment for geological data integration and 3D geological model building. Surfaces were created in Move by kriging the georeferenced lines from the geological map and cross sections. After that, geological volumes were created using the previous surfaces as top and bottom horizons. For this purpose, we used the *Create Tetravolumen between horizons* tool, using a cell size of 1 m.

3.3. Petrophysical characterization

The porous system of the different lithofacies identified in the historic quarry was studied by means of two parameters: open porosity and pore-size distribution. The open porosity (ϕ_O) was calculated using the vacuum-water-saturation test (after Anon., 1999a). Pore-size distribution was quantified by means of mercury porosimetry (MIP). The connected porosity (ϕ_{Hg}), the mean pore radius (r_M), and bulk density (ρ_{bulk}) were determined by Autopore IV 9500 Micromeritics mercury porosimetry. The pore radius interval ranged from 0.003 to 200 μm.

The capillary-absorption test was carried out in accordance with the UNE-EN 1925 (Anon., 1999a). Results were plotted as absorbed water per area of the sample against the square root of elapsed time. This representation shows two parts: the first defines water absorption; the second part defines saturation state. The Capillary Absorption Coefficient, C (expressed in $kg/m^2h^{0.5}$) was calculated from the slope of the first part of the resulting curve.

Rock durability was estimated via a salt-crystallization test. Five samples (30×30×60 mm) of each kind of lithofacies were tested using a 14 % w/w Na_2SO_4 solution, in accordance with the EN-12370 recommendations (Anon., 1999b). The rock resistance to salt weathering was quantified by means of the dry-weight loss (DWL), the alteration velocity (AV) and the alteration index (AI). AV is the final value of the derivative of the function representing the normalized weight as a function of the number of cycles (Angeli et al., 2006). AI is defined as the number of the cycle during which the first visible damage occurs (Angeli et al., 2006). Rock durability was also indirectly assessed by means of an estimator (Benavente et al., 2004). The proposed Petrophysical Durability Estimator (PDE) is defined as the ratio of parameters which quantify the pore structure of the rock to the strength of material.

Ultrasonic P-wave velocity (UPV) was measured on the same samples used for the salt-crystallization test. A Panametrics HV Pulser/Receiver 5058 PR coupled with a Tektronix TDS 3012B oscilloscope was used to perform the ultrasonic tests in transmission-reception mode. Coupled non-polarized piezoelectric transducers were employed, with a frequency spectrum of 1 MHz.

Rock strength was determined by means of Schmidt hammer after the methodology proposed in Viles et al. (2011). A minimum of 15 rebound values (R) were carried out in each tested rock in order to establish a representative value. The highest and lowest values were discarded. Uniaxial compressive strength were indirectly determined with the Schmidt hammer test using empirical relations proposed by Yagiz (2009):

$$UCS = 0.0028 \cdot R^{2.584} \quad (1)$$

This equation was adopted because it was considered the most suitable for carbonate rocks according to Andriani and Germinario (2014).

3.4. In situ rock weathering characterization

Conservation state of the architectural heritage of the Nueva Tabarca fortress was analysed at the mesoscale by visual inspection and monument mapping. The rock employed in the ashlars

of the buildings and city-walls were identified according to the rock facies previously defined in the stratigraphic sequence of *La Cantera* islet. Lithological maps of several emblematic monuments were drawn in order to show the rock varieties employed in each one and their distribution inside the building. Different deterioration patterns observed in rock ashlars were classified according to the criteria established by ICOMOS ICS glossary (ICOMOS, 2008).

4. Results

4.1. Stratigraphy of the Miocene deposits

Five lithostratigraphic units (U1-U5) are defined in the Miocene sequence of Nueva Tabarca island according to their petrographical characteristics and fossil content.

U1 – Breccias and microconglomerates. This unit is composed by 6.5 m of a succession of breccias, microconglomerates, lithoarenites and calcarenites with dispersed lithoclasts (figures 2, 3a and 3b). Contact with underlying basement corresponds to an unconformity surface that separates the Triassic materials (black limestones) and the Miocene unit. In the SG section, U1 is made up of a breccia interval 1 m thick (on the lower part) and microconglomerates (in the upper part). In both outcrops (MV and SG sections) the breccias are characterized by large, tightly packed clasts (decimetric-metric scale) of black limestone bored by *Gastrochaeonolites* isp., embedded in a greyish sandy matrix.

U2 – Calcarenite with rhodophyta algae (figure 2 and 3d). This unit presents a variable thickness (mean measured thickness around 5 m) of calcarenites (yellow-to-orange colour) with silty/clayey matrix. A small amount of scattered black limestone and metagabbro lithoclasts are identified. These are millimetre-sized and their presence gradually decrease towards the top of the unit. The fossil record includes corals, briozoos, serpulids, clypeasteroids, bivalves (*Chlamys* spp.) and fragmented and oriented red algae. The abundance of rhodoliths increase upwards, up to the point of considering the last interval of the unit as a biocalcirudite (figure 2).

U3 – Lithoarenite (figure 3e). This unit can be broadly characterized by lithoarenite beds with high density millimetric lithoclasts and small amounts of fossil components and burrows (red algae, corals, bivalves, ostreids, and *Thalassinoides*). Thickness varies from 1 to 3.5 m, approximately. In the C section, where this lithofacies is better represented, it is possible to recognize three clearly differentiated intervals. The first (1.5 m thick) is composed by breccias with decimetric/centimetric-scale clasts (lower part) and microconglomerates (upper part). The second one corresponds to a laminated lithoarenite (70 cm thick) with a low content of red algae and *Thalassinoides* isp.. Finally, the third level is a 2 m lithoarenite deposit, separated from the previous one by an undulated surface. The upper part of this level corresponds to a layer with abundant ostreids bored by *Gastrochaeonolites* isp. and *Meandropolydora* isp.

U4 - Calcarenites with interbedded biocalcirudites (figure 3f and 3g). The boundary between this unit and the previous one is marked by an undulated surface easily identified throughout the study area. The unit has a variable thickness, varying between 2.5 and 8 m. It is composed

by yellow calcarenite beds with scattered millimetric-scale clasts. Its fossil record includes corals, serpulids, echinoids (mainly attributed to *Clypeaster* genus), red algae, and highly fragmented bivalves, as well as ichnofacies (*Thalassinoides*). Three subintervals can be differentiated in the lower part of the unit (figure 2): a) lithoarenite with corals, red algae, and high amount of bored ostreids (1.2 m thick); b) calcarenite with subordinated milimetric-centimetric clasts (0.8 m thick) with a characteristic low-angle lamination; and c) biocalcirudites of rhodolithes (0.40 m thick). In the C section, where this unit is best represented, the red algae content decreases upwards. However, a distinctive layer of biocalcirudite (centrimetric-scale rhodoliths densely packed) is observed at the top of the SG section.

U5 - laminated lithoarenite (figure 3j and 3k). This unit is constituted by well-sorted lithoarenite beds with low red algae content. The thickness varies between 1 and 3 m. The presence of fragmented and oriented corals, algae, bivalves and serpulids is notable. Three intervals can be differentiated from bottom to top: a thin, hard cemented level (few cm thick); a massive and homogeneous level (around 1 m thick); and an upper interval with sub-parallel lamination.

Unit 1 exclusively outcrops in the MV section (figure 2 and 3a). Unit 2 is especially well represented in the eastern sector of the study area (SG section) (figure 2 and 3c). The boundary between units 2 and 3 is marked by an irregular erosive surface. Consequently, the thickness of the Unit 3 is the most variable, increasing eastward and westward from the SG section. Unit 4 is more developed in *La Cantera* islet (C section), reaching a thickness of 8 m. Unit 5 only outcrops in the western sections (SG and C, figure 2, 3h and 3i), being widely represented in the northern sector of the *La Cantera* islet, where part of the outcrops are currently partially submerged (figure 3i).

4.2. 3D geological model and volume quantification

Field data indicate that the quarried levels slightly dip towards the north (figure 4) in the extraction area. An angular unconformity exists between units U3 and U4, as the lower units (U2+U3) dip 10° more than the upper units. In the *La Cantera* islet the dip of all units decreases northwards along the section, making a wide and open synform. Other than stratigraphic contacts, many joints where also recognized. The contact between units U2 and U3 could be traced only in the eastern part of the study outcrop, where no extraction took place. In the quarry area, this contact is currently below sea level, so that we were unable to trace it accurately. Therefore, we decided to compute the extracted volume of these two units as a single composite stratigraphic units: U2+U3.

To quantify the extracted volume of each stratigraphic unit, we first identified and mapped the extraction areas (figure 4). Afterwards, we computed the extracted volume by subtracting the present topographic surface from the original one, prior to extraction works. The original topographic surface was initially reconstructed in 2D in 42 of the cross sections, by visually tracing interpolated envelopes between current remains of the original surface (figure 5).

These envelopes were externally limited using the coastline determined from a historical map, which was previously georeferenced in a GIS environment. Next, the 3D surface was generated by ordinary kriging, using as input data the nodes of the envelopes (figure 5) and a 0.5-m cell size. Clearly, this method implies that any original topographic irregularity in the extracted areas is neglected in the computation, and thus the calculated volumes represent only an approximation to the real extracted volumes. Further inaccuracies are related to areas lacking any remains of the original topographic surface or where topographic features cannot be unequivocally assigned to the original topographic surface. In this case, we cylindrically extended the interpolated surface using a uniform grid. Other than the present topographic surface and the interpolated original topographic surface, we also use in our volume quantification the contact between the units U3 and U4 and between U4 and U5. These surfaces were also created by ordinary kriging (0.5-m cell size), using as input the nodes of the contact traces from the cross sections.

From these surfaces, we created and computed geo-volumes of extracted material for each group of stratigraphic units (figure 6). Quantitative errors in our computation are related to the cell size of the constructed volumes. Each volume is composed of several regular tetrahedra with a 1 m edge length; as the volume is generated from surfaces, a tetrahedra adjacent to stratigraphic bounding surfaces represents a potential error of ±1 m^3. Consequently, we calculated the total volumetric error as the volume obtained after extruding the bounding surface ±1 m^3. The previously discussed inaccuracies intrinsic to our computation method were not considered as quantitative errors. We divided the study are a into three sub-areas to decrease computational times (figure 4). Our estimation indicates that a total of 36269 ±2160 m^3 of building stone were extracted, 64.5% of the blocks coming from unit U4, 10.6% from unit U5, and 22.6% from U2+U3 (24101, 3970 and 8198 m^3, respectively) (table 1).

We also computed the remaining (non-extracted) volumes of each group of stratigraphic units. In this case, we create geo-volumes using as boundary surfaces the current topographic surface, the contact between the stratigraphic units and a horizontal surface at the current sea level. Results show that a total rock volume of 61634 m^3 remains nowadays in the study area (table 1), most of this volume corresponding to the lithostratigraphic units U2 and U3 (61.3 %). Only a negligible volume of U5 remains in the study area (less than 0.5%).

4.3. Petrophysical characterization of the quarried levels

Samples from six different layers were taken from the Cantera stratigraphic section (figure 2): U2-Lalg from Unit 2, U3-L from Unit 3, U4-C (calcarenite level) and U4-C_{rod} (biocalcirudite level) from Unit 4, and U5-L (massive lithoarenite level) and U5-L_{lam} (laminated facies) from Unit 5. Sampling was focused in the Cantera section because it corresponds to the outcrops where the main historic quarries are located.

Table 2 shows the pore-size distribution quantified by means of mercury porosimetry and the values from the petrophysical tests.

In terms of durability, the softest rock is U4-C, while U5-L and U2-L_{alg} prove the most durable. According to the AI classification proposed by Angeli et al. (2007), two groups can be defined: varieties with low AI values (AI<8) (U3-L, U4-C and U4-C_{rod}) and rocks with high AI values (AI>19) (U2-L_{alg}, U5-L and U5-L_{lam}). However, with respect to the AV values found, almost all rock varieties present low velocities (less than 1%), except U4-C, which has a medium AV value (between 1 and 5). Consequently, three weathering patterns are observed. Firstly, U2-L_{alg}, U5-L and U5-L_{lam} remain practically unweathered over the whole ageing test, some slight visual deterioration detectable at the end of the test. These rock varieties are characterized by high AI and low AV values. Secondly, U3-L and U4-C_{rod} present visual damage rapidly (after only 5 cycles) but alter slowly afterwards, reaching a moderate weight loss (around 20%) at the end of the test. These samples have low values of both AI and AV. Finally, the alteration pattern of U4-C samples is characterized by early visible damage (low AI) and a progressive and rapid disintegration during the salt-crystallization test until being completely broken down after 19 cycles (high AV).

These alteration patterns depend on the water-circulation possibility, the porous system and the mechanical strength of rocks (Steiger et al., 2011). U4-C is the softest variety mainly due to its pore-size distribution (one main pore population centred between 0.1 and 1 μm) and low mechanical resistance (strength around 19.70 MPa after the Schmidt Hammer). On the contrary, the high durability of U2-L_{alg}, U5-L, and U5-L_{lam} is related to their high strength and wide pore-size distribution. Capillary Absorption Coefficient (C in table 2) also helps explain the observed rock durability due to the fact that high C values signify easy water transport through the rock. In these cases, the well-connected porous systems allow more effective evaporation and salt crystallization at or just below the stone surface, restricting the damage to slight superficial grain detachments (Cardell et al., 2003).

5. Discussion

5.1. Correlation between the volumetric analysis of the historical quarries and the building stones used in monuments

All the lithofacies studied are recognized in the architectural heritage of Nueva Tabarca fortress. They were indiscriminately used in the construction of the city-walls, the San Pedro and San Pablo church, the governor's house and the rest of local houses. However, the quantity of each rock variety used in the buildings varies significantly. It is quantified in the three monumental city-wall doors of the fortress, for example (figure 7). The original construction of the eastern entrance shows a preferred used of U5 (around 56% of the total stone volume used in the monument) and U4 (39%). The northern entrance was built with similar quantities of all units (U2=20%, U3=27%, U4=25%, and U5=28%). U3 was, however, the preferential rock variety used in the western entrance (51%), followed by U4 (29%) and U2 (18%), while U5 represents only a 2%.

The results indicate that different extraction areas supplied rock blocks to each monument studied. Three potential source areas are delimited in the figure 7 (NW, SW and E areas). They

are selected according to the correlation between the results found from both: i) the volume of each rock variety quarried in these areas; and ii) the percentage of building-stone varieties used in each monument. After the 3D geological model formulated in this study, only rock blocks of the lithostratigraphic units U4 and U5 are quarried in the NW area, being the potential source area of building stones used in the eastern city-wall door. Rock blocks from U2 and U3 were extracted mainly from the SW area (around 55%), whilst almost 40% comes from U4. Only a small quantity of building material was quarried from U5. These proportions match the lithologies identified in the ashlars of the western entrance. Finally, the E source area is the only one where all the lithostratigraphic units can be quarried in similar proportions simultaneously. This area is proposed as the supply quarry for the northern city-wall door.

Two main reasons may explain the existence of differentiated extraction areas. On the one hand, it could be due to the fact that several groups of quarry workers worked simultaneously on the construction of the Nueva Tabarca fortress and each one had been designated a different quarry front. On the other hand, although the city-walls were built in a narrow time period (less than 10 years), probably the monumental entrances are not coetaneous and the extraction area extends throughout the *La Cantera* islet, as the quarried material became exhausted.

The use of photogrammetry for the volumetric analysis of historical quarries, combined with 3D geological models, is proved to be a useful tool in works of architectural heritage research. This study constitutes a good example for other case studies. Results and methodologies can be extrapolated to other historical quarries developed on similar sedimentary deposits (Gaied et al., 2010; Mateos et al., 2011; Bednarik et al., 2014; Lanzón et al., 2014; De Kock, et al., 2017).

5.2. Rock durability and *in situ* weathering degree

In general, the most weathered variety in the monuments is U4-C, followed by U3-L. On the other hand, the least decayed ashlars in all the monuments studied correspond to U5-L_{lam} and U2-L. To quantify the erosion intensity of the different lithofacies in the monument, we calculated the mean recession depth (MRD) of ashlars in the eastern city-wall door. MRD gives the distance between both the original and the current surface of rock ashlars. MRD measured in U4-C and U3-L is 16.9 cm and 3.6 cm, respectively, whilst it is almost 0 for U5-L_{lam} and U2-L. This agrees with the durability registered by these rocks during the salt-crystallization test in laboratory (table 2).

Rock susceptibility to decay by salt crystallization is directly related to the characteristics of its porous system. Moreover, because salt growing inside pores produces stress over pore surfaces, it is reasonable to assume that stone resistance to weathering is related also to stone strength (Scherer, 2001). According to this, Benavente et al. (2004) propose a durability estimator, named PDE, based on a parameter which is dependent of the pore-size distribution and rock strength. Obtained values of PDE are shown in table 2. High values of this durability estimator indicate lower stone durability. In general terms, this theoretical estimator agreed with the observations made in both the laboratory and the monuments. Consequently, PDE can be considered a reliable durability estimator, being especially useful for heritage studies

because of the fact that it can be determined by means of non-destructive tests and/or low-invasive tests (Schmidt Hammer and mercury porosimetry in this study).

Despite that there are no univocal relationships between the observed decay forms and the lithology where they are developed, some general correlations can be made. The deterioration of U5-L, U4-C_{rod}, and U4-C is by differential erosion. This decay pattern is developed eroding preferentially soft layers included in laminated structures (U5-L_{lam}, figure 7), removing the soft matrix surrounding the hard filling of burrows (U4-C), or eliminating the matrix surrounding hard fossil components (rhodoliths in U4-C_{rod}) (figure 7). Furthermore, U4-C can show other decay patterns such as alveolization, especially in the upper parts of the monuments (figure 7). Finally, well-developed rounding forms take place preferentially in U5-L, but also in U3-L (figure 7).

Previous studies reveal that Halite crystallization and wind erosion are the main weathering agents in the Mediterranean semiarid climatic context of the fortress of Nueva Tabarca (Martínez-Martínez et al., 2017). On the one hand, wind plays a critical weathering action because it controls the salt-crystallization process (Rodríguez-Navarro et al., 1999), the abrasion by wind-blown particles (Shi and Shi, 2014), as well as the wind-driven rain impact (Erkal et al., 2012). Alveolization and differential erosion are the weathering forms typically associated to the aeolian action. These processes are especially significant in façades oriented to the East and West because they are the preferential directions of wind on the island (Martínez-Martínez et al., 2017). On the other hand, the halite crystallization aggressiveness is controlled by the local variations in relative humidity (Benavente et al., 2015). The driest periods in Nueva Tabarca correspond to the end of autumn and during the winter (Martínez-Martínez et al., 2017). Moreover, a significant decrease in the relative humidity are measured from the coast to the mainland. As a consequence, the salt-crystallization damage in building stones is geographically and temporally controlled.

5.3. Recommendations for future selection of replacement stones

Taking into account the cultural, artistic and touristic importance of the Nueva Tabarca village (Beviá and Giner Martínez, 2012), its preservation and conservation constitute a major issue, both culturally and economically. This importance emphasizes the need to understand the deterioration susceptibility of the building stones in order to define future preservation and/or conservation strategies. The use of the original building rock as replacement stone is the best option when the a monument is rebuilt or restored (Pereira and Marker, 2016). The blocks of original rock can be obtained from demolitions, ruins or directly from the historic quarry. However, the stone must be carefully selected when the original quarry shows petrographic variations because not all the original rock varieties offer the same durability and/or petrophysic characteristics.

According to the results of this study, the most suitable rock varieties for replacement works are U5-L, U5-L_{lam}, and U2-L because of both their high resistance to the artificial ageing tests and their good conservation state in the architectural heritage of Nueva Tabarca island. However, the use of U4L blocks should be avoided in places where water could come into

contact directly with the stone due to the high capillary absorption coefficient measured in this lithofacies. On the contrary, the use of U4-C must be avoided in order to guarantee a durable and efficient future restoration work.

Unfortunately, new blocks of recommended varieties (especially U5-L and U5-L_{lam}) cannot be extracted from the historic quarries. According to the data compiled, only 255 m^3 (table 1) are available today, and the small outcrops are located at a semi-submerged level in the northern area of the islet (figure 4). High rock volume of varieties from U3 and U4 can be extracted and new quarry fronts could be open in the western and southern outcrops (table 1 and figure 4). However, these rocks should be used exclusively in inside environments or very protected outer locations.

The reopening of new fronts in historical quarries is controversial where different justifications in favour and against constantly clash. On the one hand, the reopening of historical fronts allow the use of the same original building stone in the monument, contributing to maintain the conceptual homogeneity of the construction (from an architectural and historic perspective) as well as guaranteeing the perfect compatibility between new and old building materials (Rozenbaum et al., 2008; Török and Prikryl, 2010). On the other hand, it destroys historical landscapes and archaeological sites (Gaied et al., 2010). In the case of Nueva Tabarca island, the extraction of new rock blocks from *La Cantera* islet is not allowed today due to the protective measures applied to this area because of its natural landscape value. An intermediate solution in these cases is to obtain the replacement stone blocks from rubbish and from ruined buildings. However, rubble is not always available, or does not provide sufficient volume, making it necessary to use a foreign stone. Another intermediate solution is the organized management of the reopening of quarry fronts, determining the maximum extraction volume permitted as well as identifying those quarry fronts in which the environmental and the visual impact is minimum. Both the 3D geological model and the volumetric analysis of the historical quarry are fundamental tools for designing the reopening plan.

6. Conclusions

Five lithostratigraphic units are defined in the Miocene deposits of Nueva Tabarca island (SE of Spain). Differences between them were established according to: a) the content of lithoclasts; b) the percentage and type of bioclasts; c) the average size of components, and d) the presence/absence of sedimentary structures (lamination). The main identified lithologies include breccias and microconglomerates (Unit 1), massive (Unit 3) and laminated (Unit 5) lithoarenites, as well as calcarenites and biocalcirudites (Units 2 and 4). Only Units 2 to 5 outcrop in the *La Cantera* islet, corresponding to the study area where the historical quarries of Nueva Tabarca fortress are located.

With respect to durability, the softest rocks correspond to the calcarenite facies of the Unit 4, whilst rocks from Unit 2 and Unit 5 prove the most durable. The laboratory results indicated three weathering patterns : 1) rocks from Unit 2 and Unit 5, which remain practically

unweathered over the entire ageing test; 2) samples from Unit 3 and those obtained from the biocalcirudite levels from Unit 4, which present rapid visual damage but with slow progression, reaching a moderate degree of decay at the end of the test; 3) the calcarenite samples from Unit 4, characterized by early visible damage and fast disintegration. The laboratory results agree with the *in situ* weathering state observed in the monuments. Several decay forms are observed in the building stones of the Nueva Tabarca fortress: differential erosion (mainly developed on rocks from Unit 3 and 4), alveolization (in rocks from Unit 4) and rounding forms (preferentially in lithofacies of the Unit 5).

Photogrammetry and 3D geological modelling are shown to be useful tools for studying historical quarries and their connection with architectural heritage. According to the results, a total of 36269 ±2160 m^3 of building stone were extracted from the historical quarry of Nueva Tabarca. Specifically, the 64.5% of the blocks came from the unit U4, 10.6% from unit U5, and 22.6% from U2+U3. Moreover, a total rock volume of 61634 m^3 currently remains in the study area.

According to the petrophysical results presented in this paper, the most suitable rock varieties for replacement works on Nueva Tabarca monuments are those from Unit 2 and 5. However, volume quantification reveals that small quantities of these varieties outcrop today. On the contrary, high rock volume of varieties from Unit 3 and Unit 4 can be extracted and new quarry fronts could be open in the western and southern outcrops. However, the use of these rocks should be used exclusively for inside environments or well-protected outer locations.

Acknowledgements
The authors wish to thank José Manuel Pérez Burgos and Felio Lozano for their disinterested collaboration during the data collection and field works. This research was supported by projects GRE12-03 and GRE14-05 (University of Alicante).

References

Abdullah, Q., Bethel, J., Hussain, M., Munjy, R. (2013): Photogrammetric project and mission planning. In: McGlone, J.C. (Ed.), Manual of Photogrammetry. American Society for Photogrammetry and Remote Sensing.

Agisoft (2017). Agisoft PhotoScan User Manual: Professional Edition, Version 1.3. Available in http://www.agisoft.com/pdf/photoscan-pro_1_3_en.pdf

Andriani, G.F., Germinario, L. (2014): Thermal decay of carbonate dimension stones: fabric, physical and mechanical changes. Environmental Earth Sciences, 72: 2523-2539.

Andriani, G., & Walsh, N. (2003). Fabric, porosity and water permeability of calcarenites from Apulia (SE Italy) used as building and ornamental stone. *Bulletin of Engineering Geology and the Environment*, *62*(1), 77-84.

Angeli, M., Bigas, J.P., Benavente, D., Menéndez, B., Hébert, R., David, C. (2007): Salt crystallization in pores: quantification and estimation of damage. Environmental Geology, 52: 205-213.

Angeli, M., Bigas, J.P., Menéndez, B., Hébert, R., David, C. (2006): Influence of capillary properties and evaporation on salt weathering of sedimentary rocks. In: Fort, R., Alvarez de Buergo, M., Gomez-Heras, M., Vezquez-Calvo, C. (eds): Heritage, Weathering and Conservation. Taylor & Francis/Balkema, Leiden, pp 253-259.

Anon (1999a): UNE-EN 1925. Natural stone test method. Determination of water absorption coefficient by capillarity. European Committee for Standarization.

Anon (1999b): UNE-EN 12370. Métodos de ensayo para piedra natural. Determinación de la resistencia a la cristalización de sales. AENOR–CEN, 12 pp.

Baltuille, J.M., Gisbert, J., Pereira, D., Sebastián, E., Mota, M.I., Gómez Gras, D., Taboada, J., García de los Ríos, J.I., Franco, A., Fort, R. (2012): Construrock: A network at the service of Natural Stone and the Architectonic Heritage. *Abstracts of IV Global Stone Congress*, Portugal.

Bednarik, M., Moshammer, B., Heinrich, M., Holzer, R., Laho, M., Rabeder, J., Uhlir, C., Unterwurzacher, M. (2014): Engineering geological properties of Leitha limestone from historical quarries in Burgenland and Styria, Austria. Engineering Geology, 176:66-78.

Bemis, S.P., Micklethwaite, S., Turner, D., James, M.R., Akciz, S., Thiele, S.T., Bangash, H.A., (2014): Ground-Based and UAV-Based Photogrammetry: A Multi-Scale High-Resolution Mapping Tool for Structural Geology and Paleoseismology: Journal of Structural Geology, 69: 163–178 doi: 10.1016/j.jsg.2014.10.007.

Benavente, D., García del Cura, M.A., Fort, R., Ordóñez, S. (2004): Durability estimation of porous building stones from pore structure and strength. Engineering Geology, 74: 113-127.

Benavente, D., Brimblecombe, P., Grossi, C.M. (2015): Termodynamic calculations for the salt crystallisation damage in porous built heritage using PHREEQC. Environ Earth Sci, 74: 2297-2313

Beviá, M., Giner Martínez, J. (2012): Nunc Minerva postea Palas: la ciudad de Nueva Tabarca. Canelobre, 60: 114-127 (in Spanish).

Calvet, F., Zamarreño, I., Vallés, D. (1996): Late Miocene reefs of the Alicante-Elche basin, southeast Spain. In: Models for Carbonate Stratigraphy from Miocene Reef Complexes of Mediterranenan Regions.

Caracuel, J.E., Corbí, H., Giannetti, A., Monaco, P., Soria, J.M., Tent-Manclús, J.E., Yébenes, A. (2011): Paleoenvironmental changes during the Late Miocene (Messinian)-Pliocene transition: sedimentological and ichnological evidence. Palaios, 26: 754–766.

Cardell, C., Delalieux, F., Roumpopoulos, K., Moropoulou, A., Auger, F., & Van Grieken, R. (2003). Salt-induced decay in calcareous stone monuments and buildings in a marine environment in SW France. *Construction and building materials*, *17*(3), 165-179.

Cooper, B. (2010): Toward establishing a 'Global Heritage Stone Resource' designation. Episodes, 33: 38-41.

Corbí, H. (2010): Los foraminíferos de la cuenca neógena del Bajo Segura (sureste de España): bioestratigrafía y cambios paleoambientales en relación con la crisis de salinidad del Mediterráneo. Dissertation, University of Alicante

Corbí, H., Soria, J. M., Lancis, C., Giannetti, A., Tent-Manclús, J. E., & Dinarès-Turell, J. (2016). Sedimentological and paleoenvironmental scenario before, during, and after the Messinian Salinity Crisis: The San Miguel de Salinas composite section (western Mediterranean). *Marine Geology*, *379*, 246-266.

Corbí, H., Soria, J.M. (2016): Late Miocene-early Pliocene planktonic foraminifer event-stratigraphy of the Bajo Segura basin: A complete record of the western Mediterranean. Marine and Petroleum Geology, 77: 1010-1027.

De Kock, T., Turmel, A., Fronteau, G., Cnudde, V. (2017): Rock fabric heterogeneity and its influence on the petrphysical properties of a building limestone: Lede stone (Belgium) as an example. Engineering Geology, 216: 31-41.

Dreesen, R. and Dusar, M. (2004): Historical building stones in the province of Limburg (NE Belgium): role of petrography in provenance and durability assessment. Materials Characterization, 53: 273-287.

Eardley, A.J. (1942): Aerial Photographs: Their Use and Interpretation. Harper and Brothers, New York

Erkal, A., D'Ayala, D., Sequeira, L. (2012): Assessment of wind-driven rain impact, related surface erosion and surface strength reduction of historic building materials. Building and Environment, 57: 336-348.

Estévez, A., Pina, J. A., Cáliz, F., & Hervás, J. L. (1985). Isla Plana o Nueva Tabarca: Significación geológica y evolución tectónica reciente en el contexto del sector oriental de las Cordilleras Béticas. In: *La reserva marina de la Isla Plana o Nueva Tabarca (Alicante)*: 25-35. *In Spanish.*

Favalli, M., Fornaciai, A., Isola, I., Tarquini, S., Nannipieri, L. (2012): Multiview 3D reconstruction in geosciences. Computer and Geosciences, 44: 168-176.

Fronteau, G., Moreau, C., Thomachot-Schneider, C., Barbin, V. (2010): Variability of some Lutetian building stones from the Paris Basin, from characterization to conservation. Engineering Geology, 115: 158-166.

Gaied, M.E., Younès, A., Gallala, W. (2010): A geoarchaeological study of the ancient quarries of Sidi Ghedamsy island (Monastir, Tunisia). Archaeometry, 52 (4): 531-549.

García-García, F., Corbí, H., Soria, J.M., Viseras, C. (2011): Architecture analysis of a river flood-dominated delta during an overall sea-level rise (Early Pliocene, SE Spain). Sedimentary Geology, 237: 102–113.

Graue, B., Siegesmund, S., Middendorf, B. (2011): Quality assessment of replacement stones for the Cologne Cathedral: mineralogical and petrophysical requirements. Environmental Earth Sciences, 63: 1799-1822.

Hyslop E.K. (2004): The performance of replacement sandstone in the new town of Edinburgh. Edinburgh: Historic Scotland Research Report. Edinburgh: Historic Scotland.

ICOMOS-ISCS (2008): Illustrated glossary on stone deterioration patterns. http://international.icomos.org/publications/monuments_and_sites/15/pdf/Monuments_and_Sites_15_ISCS_Glossary_Stone.pdf

James, M.R., Robson, S. (2014): Mitigating systematic error in topographic models derived from UAV and ground-based image networks: Earth Surface Processes and Landforms, 39: 1413–1420, doi: 10.1002/esp.3609.

James, M.R., Varley, N. (2012): Identification of structural controls in an active lava dome with high resolution DEMs: Volcán de Colima, Mexico: Geophysical Research Letters, 39: 22 L22303, doi: 10 .1029 /2012GL054245 .

Kampschuur, U., Simon, O.J. (1969): Sur la géologie de l'ile de Tabarca (prov. d'Alicante, Espagne). C.R. Som. S. G. F., t.2, p. 37.38.
Krauss, K. (1993). Photogrammetry. In: Fundamentals and Standard Processes, vol. 1. Dümmlers.

Lanzón, M., cnudde, V., De Kock, T., Dewanckele, J., Piñero, A. (2014): X-ray tomography and chemical-physical study of a calcarenite extracted from a Roman quarry in Cartagena (Spain). Engineering Geology, 171: 21-30.

Mateos, R.M., Durán, J.J., Robledo, P.A. (2011): Marès Quarries on the Majorcan Coast (Spain) as Geological Heritage Sites. Geoheritage, 3: 41-54.

Micheletti, N., Chandler, J.H. and Lane, S.N. (2015): Structure from motion (SFM) photogrammetry. IN: Clarke, L.E. and Nield, J.M. (Eds.) Geomorphological Techniques (Online Edition). London: British Society for Geomorphology. ISSN: 2047-0371, Chap. 2, Sec. 2.2.

Montenat, M. (1977): Les bassins néogènes et quaternaires du Levant d' Alicante à Murcie (Cordillères Bétiques orientales, Espagne). Stratigraphie, paléontologie et évolution dynamique. Docum. Lab. Géol. Fac. Sci. Lyon. 69.

Montenat, M., Ott dÈstevou, P., Coppier, G. (1990): Les bassins neógènes entre Alicante et Cargatena. Doc. Et Trav. I.G.A.L., 12-13: 313-368.

Niethammer, U., James, M.R., Rothmund, S., Travelletti, J., Joswig, M. (2012): UAV based remote sensing of the Super-Sauze landslide: evaluation and results. Eng. Geol., Integration Technol. Landslide Monit. Quant. Hazard Assess. 128, 2e11. http://dx.doi.org/10.1016/j.enggeo.2011.03.012.

Pereira, D. and Marker, B. (2016): The value of original natural stone in the context of architectural heritage. Geosciences, 6 (13): 1-9

Pereira, D., Baltuille, J.M., Cooper, B.J. (2013): Documenting the architectonic heritage: the best way of preserving it. In: Science and Technology for the Conservation of Cultural Heritage. Rogerio-Candelera, Lazzari and Cano (Eds). Taylor and Francis Group. London. Pp 411-414.

Pillmore, C.L. (1964): Application of high-order stereoscopic plotting instruments to photogeologic studies. In: Procedures and Studies in Photogeology, Geological Survey Bulletin 1043-B. U.S. Department of the Interior, Geological Survey, Washington, D.C, pp. 22e34.

Rodriguez-Navarro, C., Doehne, E., Sebastián, E. (1999): Origins of honeycomb weathering: The role of salts and wind. GSA Bulletin, 111.

Rozenbaum, O., Barbanson, L., Muller, F. and Bruand, A. (2008): Significance of a combined approach for replacement stones in the heritage buildings' conservation frame. CR Geoscience, 340: 345-355.

Sasse, H.S. Snethlage, R. (1996): Methods for the evaluation of stone conservation treatments. In: Report of Dahlem Workshop on Saving Our Architectural Heritage. Baer, N.S., Snethlage, R. (Eds.). pp. 223-243.

Scherer, G.W., Flatt, R., Wheeler, G. (2001): Materials science research for the conservation of sculpture and monuments. MRS Bulletin, 26: 44-50.

Shi, X.J., Shi, X.F. (2014): Numerical prediction on erosion damage caused by wind-blown sand movement. European Journal of Environemtnal and Civil Engineering, 18: 550-566.

Smith, M.J., Chandler, J., Rose, J. (2009): High spatial resolution data acquisition for the geosciences: kite aerial photography. Earth Surf. Process. Landforms 34, 155e161. http://dx.doi.org/10.1002/esp.1702.

Soria, J.M., Alfaro, P., Fernández, J., Viseras, C. (2001): Quantitative subsidence-uplift analysis of the Bajo Segura Basin (eastern Betic Cordillera, Spain): tectonic control on the stratigraphic architecture. Sedimentary Geology, 140: 271–289.

Soria, J.M., Caracuel, J.E., Corbí, H., Dinarès-Turell, J., Lancis, C., Tent-Manclús, J.E., Viseras, C., Yébenes, A. (2008a): The Messinian-Early Pliocene stratigraphic record in the southern Bajo Segura Basin (Betic Cordillera, Spain). Implications for the Mediterranean salinity crisis. Sedimentary Geology, 203: 267–288.

Soria, J.M., Caracuel, J.E., Corbí, H., Dinarès-Turell, J., Lancis, C., Tent-Manclús, J.E., Yébenes, A. (2008b): The Bajo Segura Basin (SE Spain): implications for the Messinian Salinity Crisis in the Mediterranean margins. Stratigraphy, 5: 259–265.

Steiger, M., Charola, A.E., Sterflinger, K. (2011): Weathering and deterioration. In: *Stone in architecture*. Springer Berlin Heidelberg: 227-316.

Stumpf, A., Malet, J.-P., Kerle, N., Niethammer, U., Rothmund, S. (2013): Image-based mapping of surface fissures for the investigation of landslide dynamics. Geomorphology 186, 12e27. http://dx.doi.org/10.1016/j.geomorph.2012.12.010.

Török, A., and Prikryl, R. (2010): Current methods and future trends in testing, durability analyses and provenance studies of natural stones used in historical monuments. Engineering Geology, 115: 139-142.

Viles, H., Goudie, A., Grab, S., Lalley, J. (2011): The use of the Schmidt Hammer and Equotip for rock hardness assessment in geomorphology and heritage science: a comparative analysis. Earth Surface Processes and Landforms, 36: 320-311.

Westoby, M.J., Brasington, J., Glasser, N.F., Hambrey, M.J., and Reynolds, J.M. (2012) 'Structure-from-Motion' photogrammetry: A low-cost, effective tool for geoscience applications: Geomorphology, 179: 300–314.

Yagiz, S. (2009): Predicting uniaxial compressive strength, modulus of elasticity and index properties of rocks using the Schmidt hammer. Bulletion of Engineering Geolology and Environment,68: 55–63

Figure captions

Figure 1: Location map and geological setting of the Nueva Tabarca island.

Figure 2: Stratigraphy of the Miocene sequence of Nueva Tabarca island. a) Moll Vell (MV), San Gabriel (SG) and Cantera (C) stratigraphic sections (red stars indicate the sampled levels for petrophysical characterization). b) Cartography of the lithostratigraphic units identified in the different studied sections. Green boxes 'A', 'C', 'H' and 'I' indicate the location of the corresponding pictures showed in figure 3 ('a', 'c', 'h' and 'i', respectively).

Figure 3: Photographs of the different lithoestratigraphic units. (a) and (b) correspond to the outcrops of Unit 1 in the MV Section. (c) shows the outcrops of Unit 2, 3 and 4 in the SG study area. Photographs (d), (e), (f) and (g) illustrate the main lithologies recognized in these units. (h) and (i) show the contact between Unit 4 and Unit 5 in the SG study area (h) and in the *La Cantera* islet (i). Photographs (j) and (k) correspond to detailed photographs of the main lithologies recognized in Unit 5.

Figure 4: Geological map of the historic quarry of Nueva Tabarca Island. Grey lines indicate cross section used for reconstruction of the original topographic surface and 3D geological model. Extraction areas are also indicated (dotted) together with sub-areas for volume computation. Grid represents UTM coordinates (Zone 30N).

Figure 5: *a* and *b*: examples of cross sections used for reconstruction of the original topographic surface and 3D geological model (location in figure 4). Red lines are the envelopes by visual interpolation between present remains of the original surface. *c*: 3D view of present topography of sub-area 1 (grey mesh) with all the envelopes traced. *d*: 3D view of original topographic surface reconstructed by kriging the envelopes nodes (red mesh) and the present topography of sub-area 1 (grey mesh).

Figure 6: example of reconstructed extracted volume from sub-area 3. The yellowish mesh represents the stratigraphic contact between units U2+U3 and U4. Grey lines in the extracted volume (also in yellow) represent the $1m^3$ tetrahedrals used for reconstruction. Grey mesh represents the present topographic surface.

Figure 7: a) location of the three studied city-wall entrances and their respective proposed extraction areas (see text). b) lithological mapping of the three city-wall doors showing different examples of decay patterns. The white polygons in northern and western entrances indicate non-studied rock varieties (replaced blocks). The photographies in the lower left corner are not georeferenced because they were taken from ashlars of the city-wall surrounding the eastern entrance. These photographs are included in this figure due to the exemplariness of the referred decay forms.

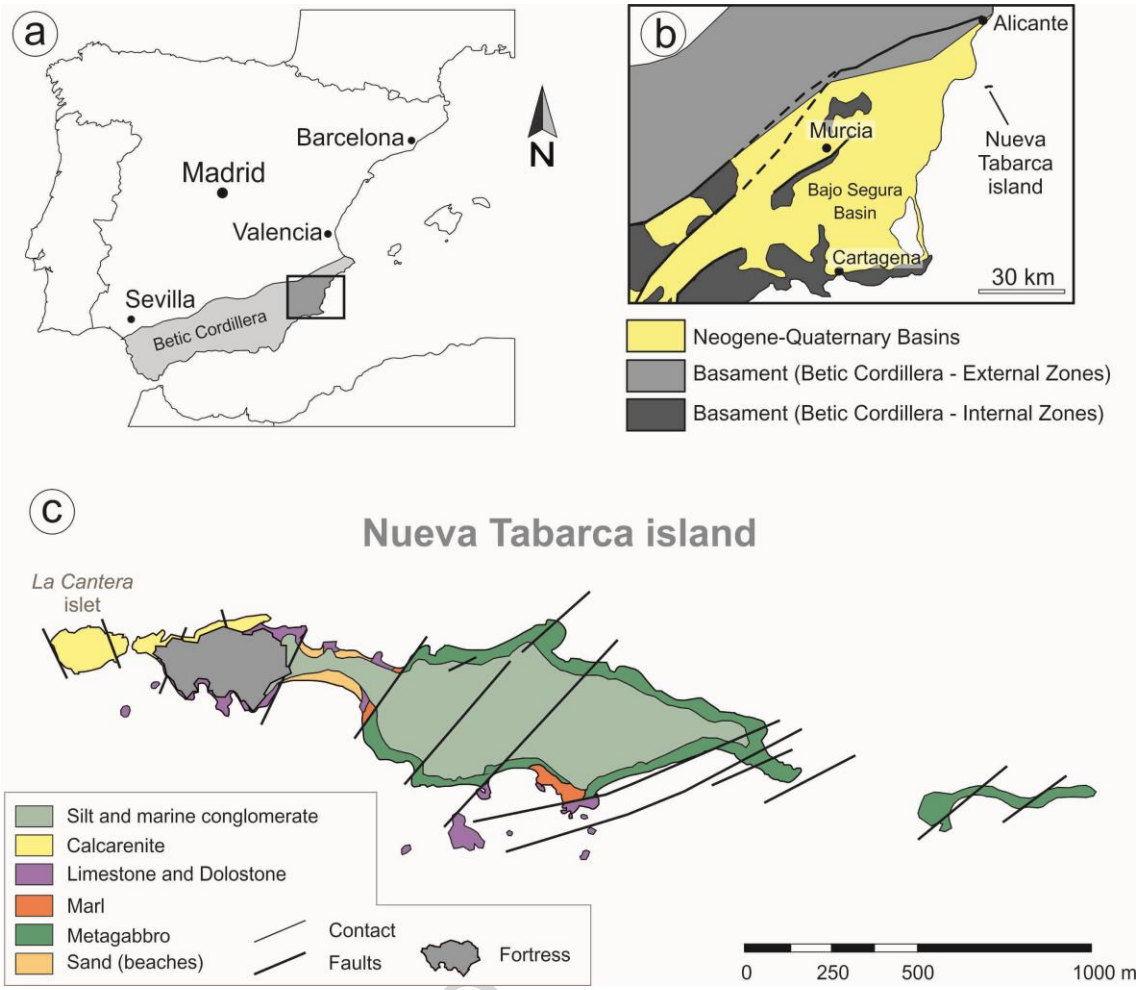

Fig. 1

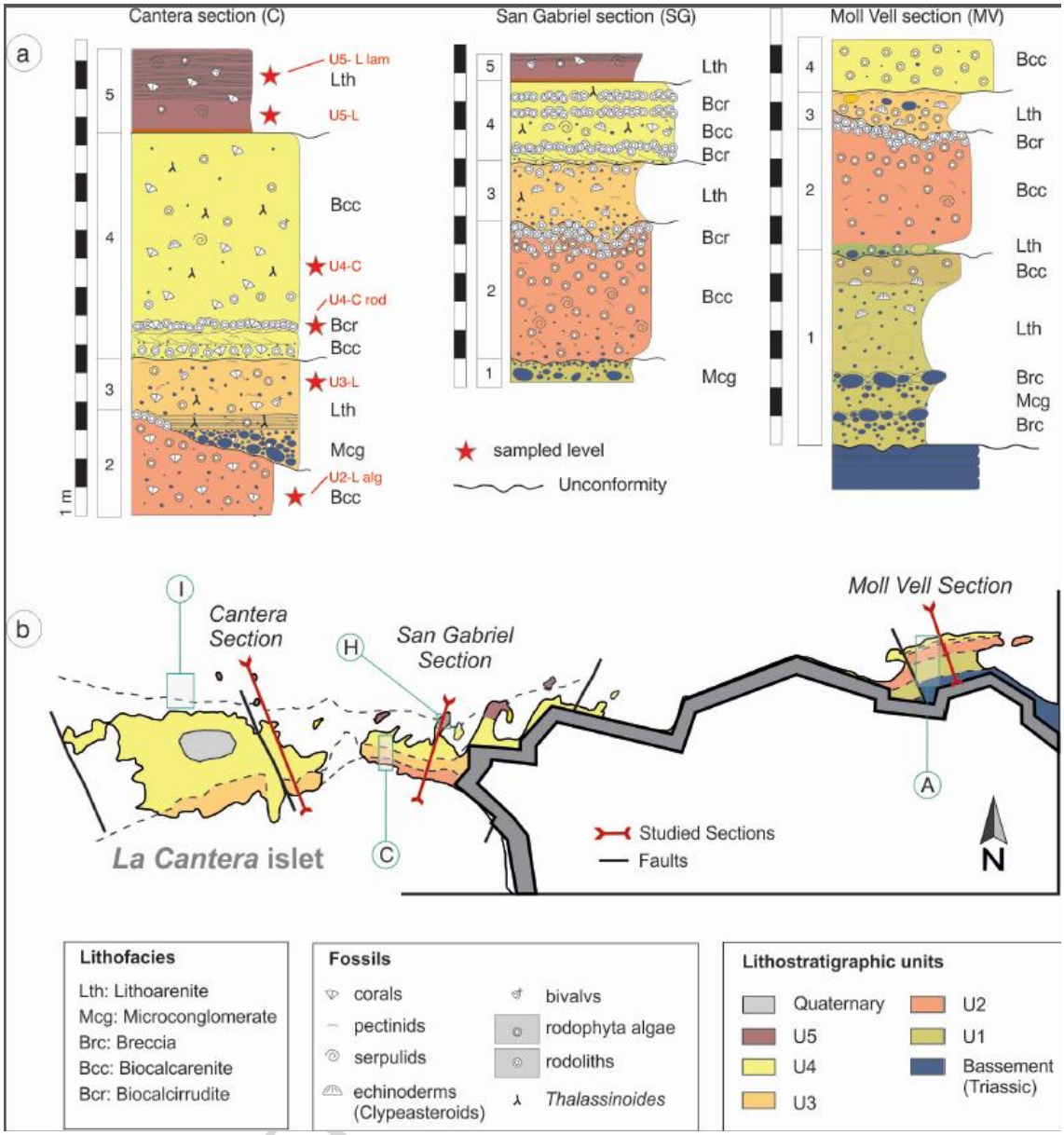

Fig. 2

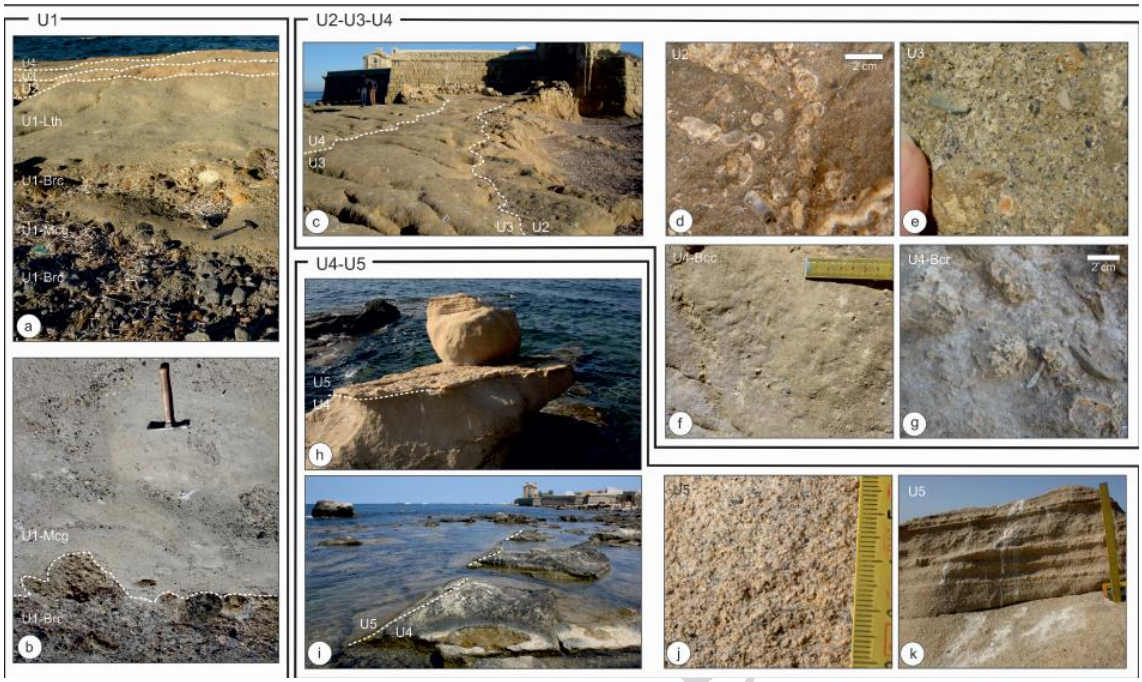

Fig. 3

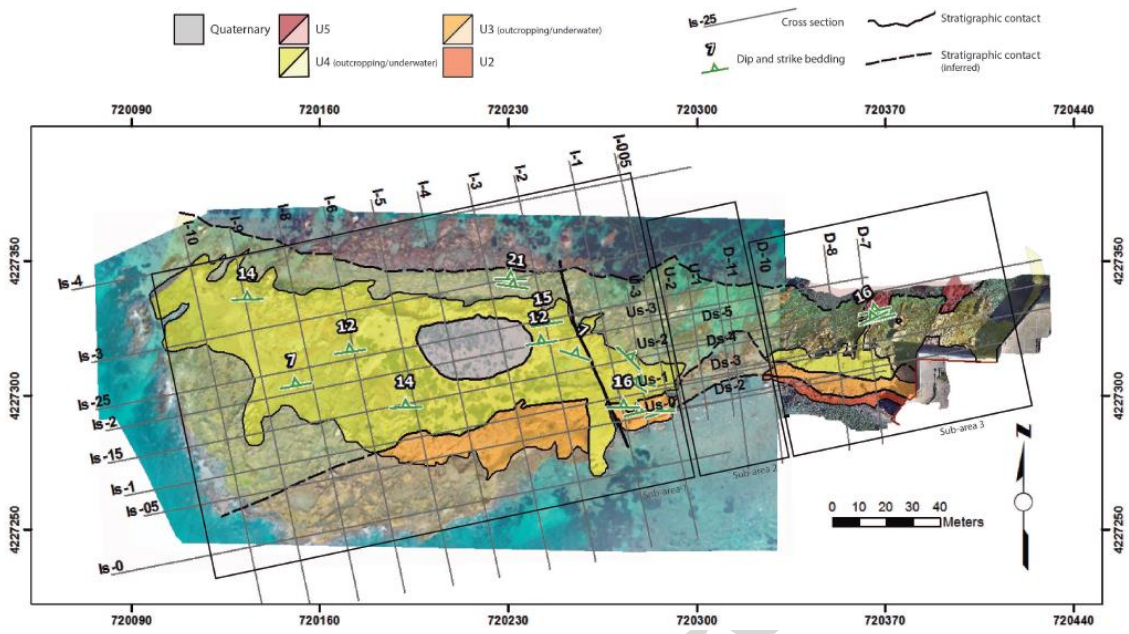

Fig. 4

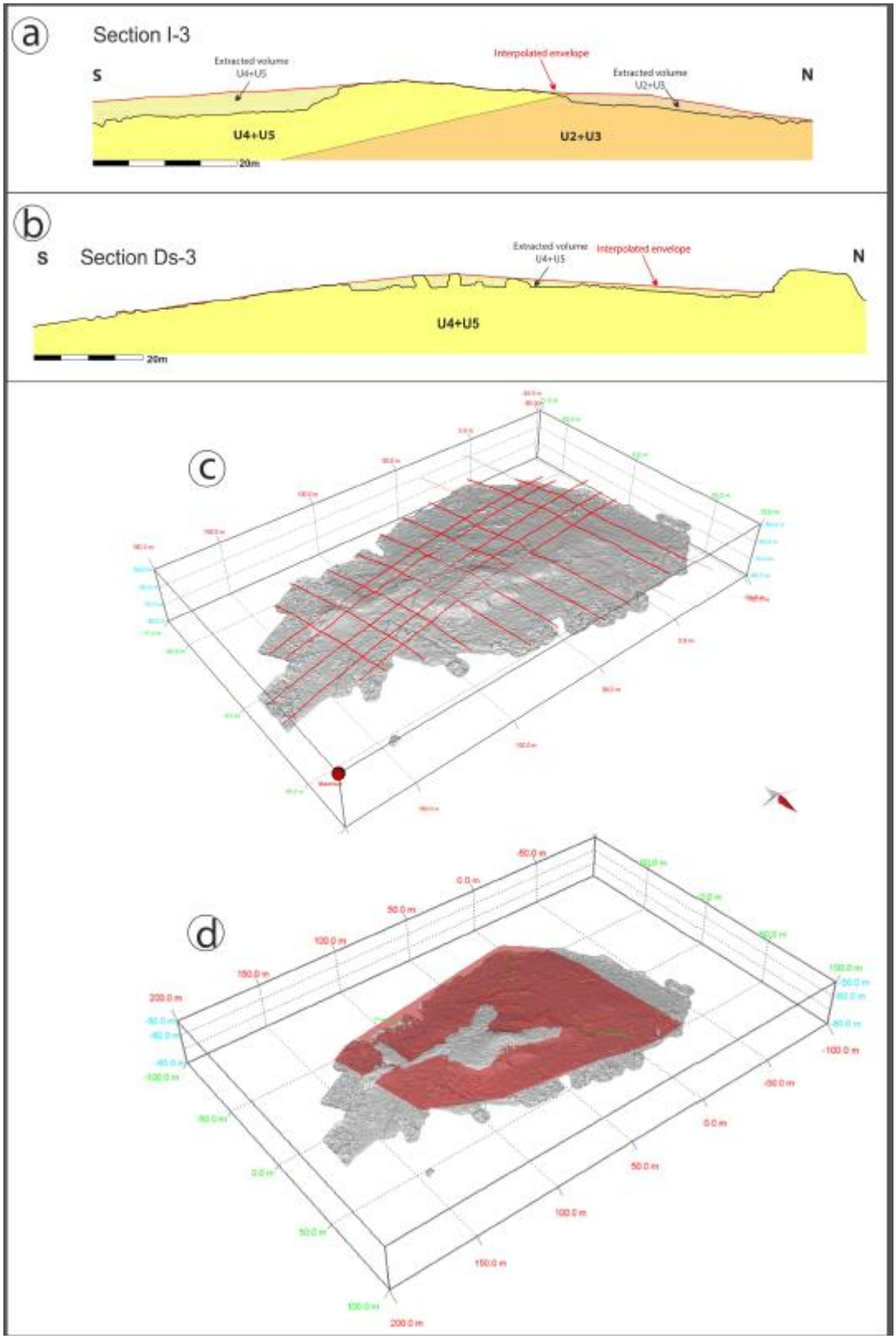

Fig. 5

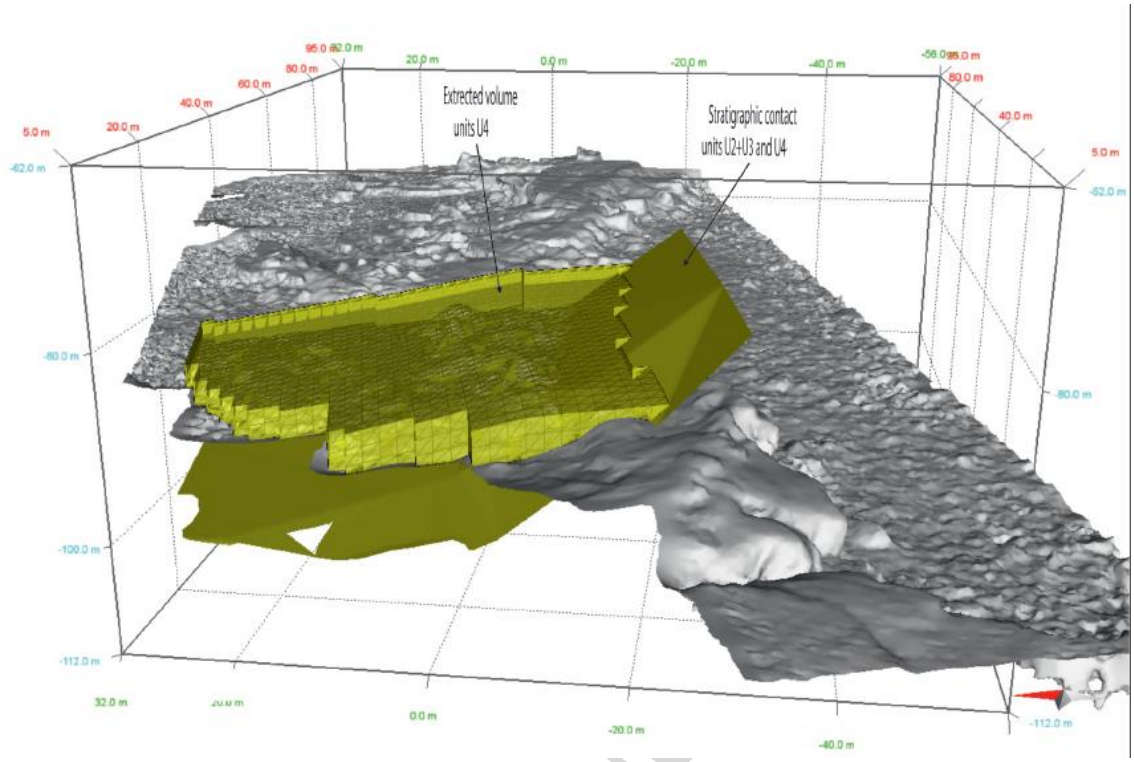

Fig. 6

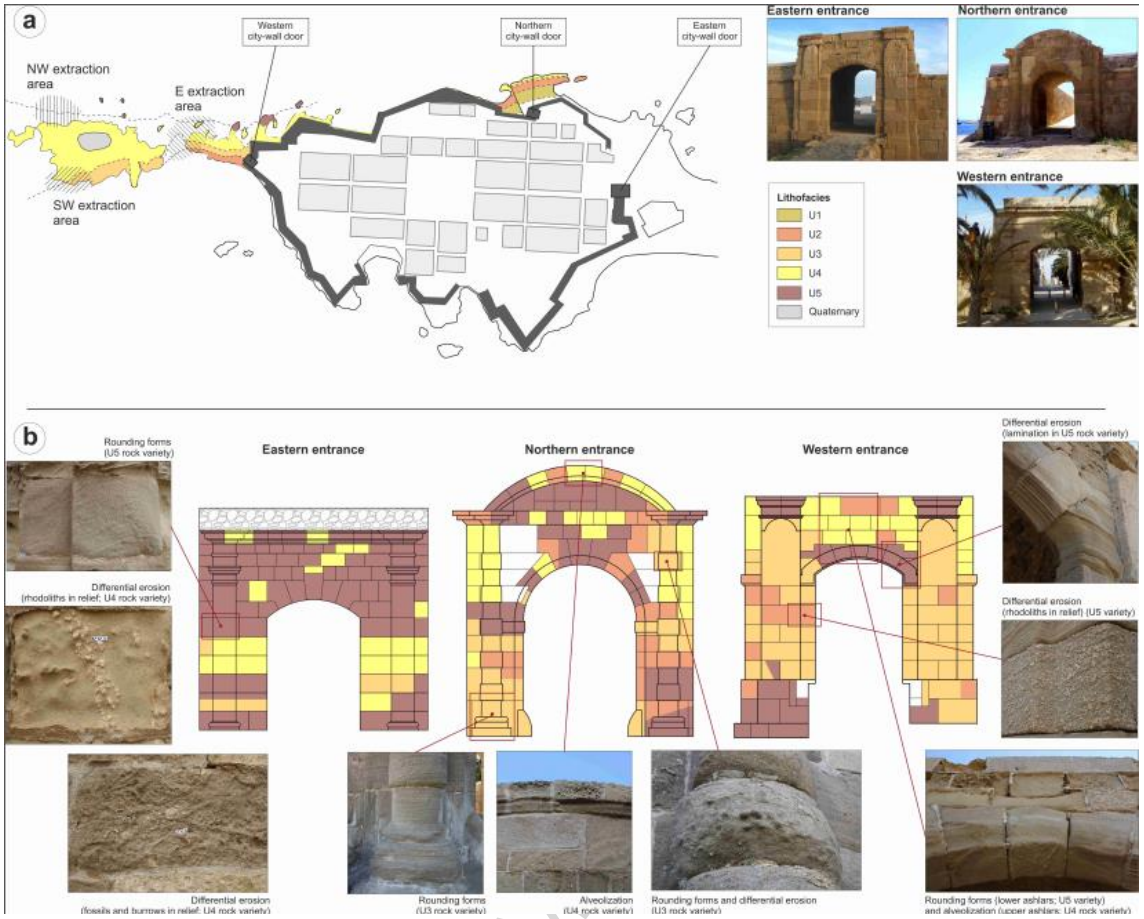

Fig. 7

Table 1. Extracted and remaining volumes of rocks. The studied area has been subdivided in partial areas 1, 2 and 3 (see figure 4 and explanation in the text).

		Extracted Volume			
		Partial volume (Sub-Areas)			**Total**
		1	2	3	
Total	[m^3]	31220 ±1654	2902 ±176	2147 ±330	36269 ±2160
U2+U3	[m^3]	7380 ±827	294 ±88	524 ±165	8198 ±1080
	[%]	23.6 ±5.3	10.1 ±6.06	24.4 ±15.4	21.9 ±6.0
U4	[m^3]	20269 ±413	2608 ±88	1224 ±88	24101 ±501
	[%]	64.9 ±3.8	89.9 ±2.2	57.0 ±6.1	64.5 ±3.5
U5	[m^3]	3571 ±414	0 ±0	399 ±87	3970 ±480
	[%]	11.4 ±3.4	0.0 ±0.0	18.6 ±6.3	10.6 ±5.2

		Remaining Volume			
		Partial volume (Sub-Areas)			**Total**
		1	2	3	
Total	[m^3]	54465 ±1540	6572 ±72	597 ±33	61634 ±1980
U2+U3	[m^3]	33368 ±721	1827 ±82	231 ±101	35426 ±2204
	[%]	61.3 ±3.0	27.8 ±2.7	38.7 ±5.4	57.5 ±3.5
U4	[m^3]	20884 ±308	4745 ±22.7	324 ±60.9	25953 ±1320
	[%]	37.7 ±10.1	72.2 ±7.6	49.8 ±10.3	42.1 ±19.3
U5	[m^3]	213 ±10.3	0 ±0	42 ±5.9	255 ±86
	[%]	1.0 ±0.3	0.0 ±0.0	11.4 ±3.4	0.4 ±0.1

Table 2. Mineral content, pore size distribution and petrophysic parameters of the studied rocks. ρ_{bulk}: bulk density; ϕ_o: Open porosity; ϕ_{Hg}: connected porosity; r_M: mean pore radius; C: Capillary Absorption Coefficient; R_{SH}: Rebound value obtained with Schmidt Hammer; UCS_{SH}: strength after equation 1; UPV: ultrasonic P-wave velocity; DWL: dry weight loss after salt crystallization test; AI: alteration index; AV: alteration velocity.

	U2-L_{alg}	**U3-L**	**U4-C**	**U4-C_{rod}**	**U5-L**	**U5-L_{lam}**
Porous system characterization						
ρ_{bulk} [g/cm3]	2.17	2.05	2.34	2.12	2.07	2.08
ϕ_o [%]	20.12	22.91	15.81	21.72	24.65	21.59
ϕ_{Hg} [%]	18.30	19.86	15.13	24.09	23.90	22.28
r_M [µm]	0.17	0.10	0.10	0.26	0.21	0.37
Pore size distribution [µm]						
<0.01	3.57	4.92	4.47	0.68	1.60	0.77
0.01 - 0.1	13.92	14.10	25.74	22.53	11.44	9.36
0.1 - 1	33.37	26.93	60.05	55.82	32.31	36.90
1 - 10	38.05	49.08	4.07	15.76	35.39	46.85
10 - 100	11.09	4.98	5.68	5.22	19.25	6.12
>100	0.00	0.00	0.00	0.00	0.00	0.00
Hydric properties						
C [$Kg/m^2h^{0.5}$]	11.65	9.01	2.88	4.67	8.01	5.04
Mechanical properties						
R_{SH}	31.85	40.65	30.82	34.15	41.50	42.15
UCS_{SH} [MPa]	21.44	40.27	19.69	25.67	42.48	44.22
UPV [km/s]	1.83	2.55	1.85	2.04	1.79	2.63
Durability						
DWL [%]	0.31	27.63	81.87	18.27	0.25	2.45
AI [cycle]	-	5	3	5	-	30
AV [%/cycle]	0.02	0.92	4.31	0.61	0.01	0.01

Highlights

- Stratigraphic description of complex sedimentry Miocene sequence is presented.
- Durability of selected lithofacies is explained after hydric/mechanical properties.
- Building stones in monuments are classified according to quarried stratigraphic le vels
- 3D models are applied to the volumetric analysis of the historic quarry
- Replacement stones are selected according to petrophysical and volumetric criteria.